JMEPEG (2004) 13:24-31
DOI: 10.1361/10599490417551

1059-9495/$19.00

Structural Evolution and Superplastic Formability of Friction Stir Welded AA 2095 Sheets

H.G. Salem, A.P. Reynolds, and J.S. Lyons

(Submitted 18 August 2003; in revised form 31 October 2003)

Friction stir welding was used to join superplastic AA 2095 sheets. The effect of welding rate on the grain size distribution and grain boundary misorientations in the stir zone was investigated. The superplastic behavior of the weld nugget parallel to the welding direction was also characterized at 495 °C and strain rates from 10^{-4} s^{-1} to 10^{-2} s^{-1}. Increasing the welding rate during friction stir welding augmented the formation of a fine-equiaxed high-angle grain boundary structure within the stir zone. Increasing intensity of plastic straining during friction stir welding resulted in enhanced properties during subsequent superplastic formation. The maximum strain-to-failure was obtained for the weld made at a tool speed of 1000 rpm and a weld rate of 4.2 mm/s when tested at a superplastic forming strain rate of 10^{-3} s^{-1}.

Keywords cold and hot welds, friction stir welding, microstructure, superplastic behavior.

1. Introduction

The intense plastic straining associated with friction stir welding (FSW) can create very fine grain structures in the stirred region of the weld nugget. Due to the frictional effect as well as shear deformation, the material undergoes localized heating, and hence, relative softening, which facilitates plastic deformation. The temperature in the weld has been suggested to be around 450 °C for Al-alloys. Recrystallization taking place within the stirred region was responsible for the refinement of the structure to 0.5 μm in a 2024-aluminum (Al) alloy.[1,2] Grain refinement depends on the welding rate, rotational speed of the tool, pin geometry, thickness of the work piece, and the material processed. Such grain refinement can be sufficient to create a material amenable to high strain rate superplasticity in plates with initially coarse grain structures.[3,4]

Al alloys like 2095 are thermomechanically processed to obtain an ultrafine grain structure suitable for superplastic forming (SPF) by design. The retention or enhancement of superplasticity of these alloys through friction stir welding is therefore of interest. It has been shown that Weldalite alloy sheets retain their superplastic properties after being friction stir welded if they are tested transversely to the weld direction.[5,6] This paper explores the superplastic behavior parallel to the welding direction. Specifically, the effects of the different friction stir welding rates on the microstructural evolution and superplastic behavior of AA 2095 dynamically recrystallized superplastic sheets are investigated.

H.G. Salem, Dept. of Mechanical Engineering, American University in Cairo, P.O. Box 2511, Cairo, Egypt, e-mail: hgsalem@aucegypt.edu; **A.P. Reynolds** and **J.S. Lyons**, Dept. of Mechanical Engineering, University of South Carolina, Columbia, SC 29208. Contact e-mail: lyons@sc.edu.

2. Material and Procedure

The alloy selected for the current work was Weldalite 2095 Al-Cu-Li base alloy received in the form of dynamically recrystallized sheets 1.63 mm in thickness and with an average grain size of 3 μm. Weldalite is a trademark of the Reynolds Aluminum (Reynolds Metal Company, Richmond, VA). The alloy composition is Al-1.14% Li-4.6% Cu-0.38% Mg-0.17% Zr-0.33% Ag-0.03% Ti-0.02% Zn, and minor additions of Fe and Si. The sheets were friction stir welded using a tool with pin and shoulder diameters of 3.8 and 10 mm, respectively, and a tool rotation speed of 1000 rpm. Three different welding rates of 2.1, 3.2, and 4.1 mm/s were investigated. Figure 1(a) shows a schematic representation for the tool rotation direction, where the right-and left-sides of the weld center are consistent with the retreating and advancing sides of the rotating tool, respectively. Also Fig. 1(a) shows that rectangular strips prepared for butt joining using friction stir welding were cut from the sheets so that the welding direction was parallel to the rolling direction.

Since alloy 2095 has a rapid natural aging response,[7] the sheets were naturally aged 3 months after friction stir welding before testing. The microstructure after natural aging was characterized with optical microscopy and with orientation imaging microscopy. The microstructural samples were cut from the cross section perpendicular to the welding direction and were etched by Keller's reagent. The orientation-imaging microscope (OIM) was attached to a PHILIPS XL-30 scanning electron microscope (SEM) (Philips, Hillsboro, OR) operating at 25 KV. The OIM was used to evaluate grain size distribution and grain boundary misorientation for the friction stir welded sheets at the different welding rates and for the base metal. The OIM step size was 1 μm (Fig. 1b). The solid squares shown in Fig. 1b show the locations of the OIM studies. These allowed an investigation of the effect of the local plastic flow on the microstructural evolution of the welded sheets. The grain size distribution with the weld nuggets and the base metal were also measured by the linear intercept method using LIECA image analysis software (Leica Microsystems Ltd., Heerbrugg, Switzerland). The superplastic behavior of the as-received and the welded sheets was characterized through conducting uniaxial tensile testing without backpressure using specimens cut par-

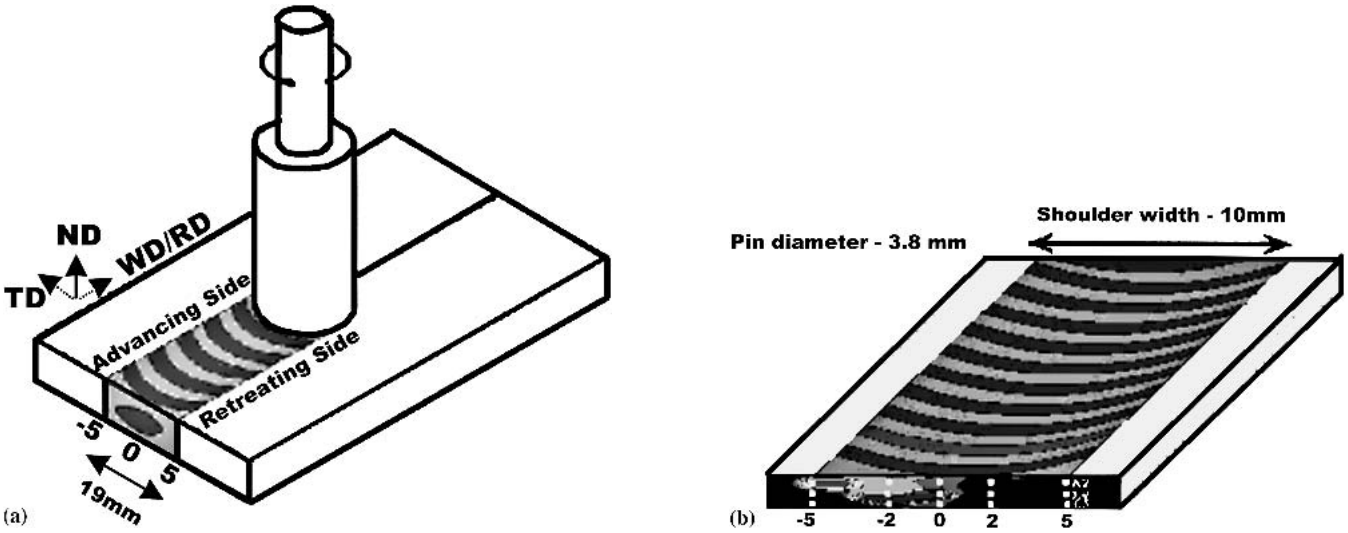

Fig. 1 **(a)** Schematics of the plate geometry showing the welding operation and **(b)** the locations of microstructural examinations shown by solid squares on the sheet's cross-section

allel (i.e., longitudinal) to the welding direction. The superplastic tensile specimen gage length, width, and thickness were 16, 5, and 1.6 mm, respectively. Constant true strain rate testing was conducted at strain rates from 10^{-4} to 10^{-2} s^{-1}. Reported total strain (elongation-to-fracture) for the base metal before and after welding was based on the average of at least two tests. The strain rate sensitivity was approximated at several strain values from tests run at different constant strain rates.

3. Results

3.1 Microstructural Evolution

Detailed optical and transmission electron microscopy results of the as-received material were previously reported.[5,7] The microstructure included elongated grains several hundred microns long and few microns wide in the rolling direction representing the as cast structure. The elongated cast grains were composed of fine pancake shaped subgrains about 4.0 μm long and 1.2 μm wide, in addition to a fine equiaxed structure with grains about 3 μm in average size, as shown in Fig. 2. The as received alloy contained a variety of coarse and fine second phase particles such as θ(Al_2Cu), T_B ($Al_{15}Cu_8Li$), S′(Al_2CuMg), δ′(Al_3Zr), and β′(Al_3Li). Detailed information of the base metal microstructure and analysis of the second phase particles' morphology has been presented in Ref 7.

Microstructural investigation using optical microscopy for the welded sheets within the weld nugget for all three welding rates revealed the formation of similar macro and microstructures with slight variations. Accordingly, the sheets welded at the 2.1 and 4.1 mm/s were chosen for detailed analysis in the current section. Based on evidence that the heat input to the weld increases with decreasing welding rate using the same rotational speed, the welds at 2.1 and 4.2 mm/s are referred to as the hot and cold welds, respectively.

Similar to observations made by other researchers, the weld zone widened near the upper surface, due to its exposure to

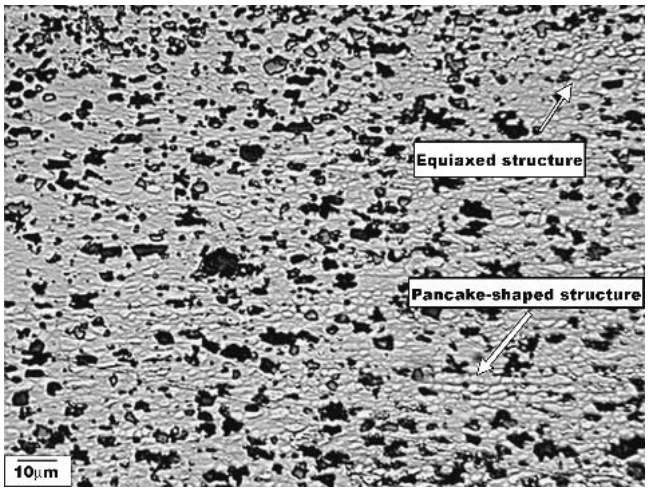

Fig. 2 Optical photomicrograph showing the equiaxed and pancake shaped structures (indicated by arrows) in the base metal

excessive heating by friction and plastic flow at the shoulder-sheet-interface during welding.[8] However, the current weld zones did not show the elliptical nugget shape reported for other alloys,[1,9-11] which could be related to the small thickness of the investigated sheets. Friction stir welding formed a heterogeneous structure through the sheet thickness, as shown in Fig. 3. Here, the advancing side is on the left and the retreating side is on the right. The microstructurally developed regions can be divided into 4 distinct zones: the stir zone along the weld centerline, a swirl zone extending towards the advancing side of the tool and within the stir zone, a thermomechanically affected zone (TMAZ) on either sides of the weld and a heat affected zone (HAZ) surrounding the TMAZ. Similar observations were made by Posada et al., on a stainless steel.[9] The stir zone corresponds to the region covered by the 3.8 mm diameter rotating pin and hence is located from +2 mm on the retreating side to −2 mm on the advancing side. The stir zone

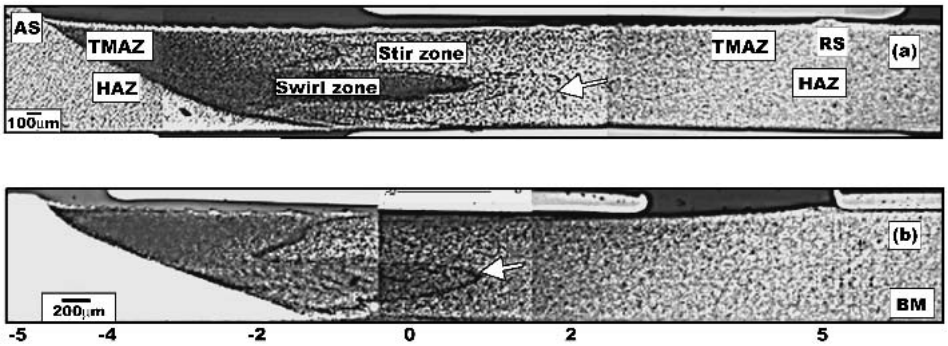

Fig. 3 Optical micrographs showing the flow pattern in the nuggets after welding at 1000 rpm and feed rates of **(a)** 2.1 mm/s and **(b)** 4.2 mm/s.

shows a lack of symmetry along the centerline of the weld. For all three welding conditions, intense plastic deformation and material flow was more pronounced on the advancing side, as shown in Fig. 3. The swirl zone is a region formed within the stir zone that shows evidence of the material flow within the pin threads. This was more pronounced in the cold weld. It appears that the pin threads directed the material down to the bottom of the pin and also fragmented the coarse particles in the microstructure.

The hot weld shown in Fig. 3(a) differs from the cold one shown in Fig. 3(b), primarily in the shape and size of the swirl zone. Sharp delineation between the swirl zone and the surrounding parts of the stir zone was observed in the cold weld. The swirl zone in the hot weld extended more horizontally across the weld nugget. The approximate widths of the swirl zones for the hot and cold welds are 5 and 4.3 mm, respectively. The hot weld showed aligned fine particles starting at the top surface of the swirl zone and extending toward the retreating shoulder to a distance of 2 mm on the right of the weld nugget center, as indicated by the arrow in Fig. 3(a).

The TMAZ region extends on both sides of the weld towards both shoulders where less material flowed and lower temperatures occurred than in the stir zone. From Fig. 3, it was observed that the TMAZ on the advancing shoulder was more pronounced than on the retreating one. In general, friction stir welding produced grain sizes that varied between 2.6 and 4.5 μm and 2.2 and 3.6 μm at different locations across the weld nugget for the hot and cold welds, respectively.

The optical micrographs shown in Fig. 4 represent microstructures developed at different locations within the weld nugget of the hot weld. Following the notation shown in Fig. 1(b), the displayed four microstructures shown in Fig. 4(a-d) represent (−1, 1.0), (−1, 1.2), (1, 1.0), and (6, 1.0), respectively.

Figure 4(a) shows the developed microstructure during FSW at (−1, 1.0), which corresponds to the swirl zone and the region just above it. A fine equiaxed structure associated with very fine particles and almost no trace of the coarse ones is developed within the swirl zone. On the other hand, coarse particles can be observed above (Fig. 4a) and below (Fig. 4b) the swirl zone, with relatively higher volume fraction below the swirl zone. Figure 4(c) shows the microstructure of the swirl zone where it terminates on the right hand side of the weld nugget and extends towards the retreating side. For comparison, Fig. 4(d) shows the microstructure of the base metal at 6 mm from the weld nugget center on the retreating side and 1.0 mm from the top surface of the sheet. A mixture of equiaxed grains of 4 μm in average size and pancake-shaped grains about 4.2 μm long and 1.5 μm wide are observed. The measured structure size is slightly coarser than that measured in the base metal sheets prior to welding (Fig. 2). This indicates that regions on either side of the weld nugget are slightly affected by the heat generated during FSW.

OIM analysis was performed on the base metal and on the hot and cold-welds. Grain size distribution and misorientation angle histograms within the weld nugget were determined. Low angle boundaries are defined as boundaries with less than 15° in misorientation. High angle boundaries are defined as boundaries with more than 15° in misorientation. Misorientation angles between the grain boundaries within the stir zone for the hot weld are shown in Fig. 5. In the stir zone and above the swirl zone the average grain size measured by OIM was 4.0 μm, and below the swirl zone the average grain size was 3.2 μm, which agrees with the measured grain size using linear intercept technique. Regions below the swirl zone had a relatively higher fraction of low-angle boundaries compared with regions above and within the swirl zone. In particular, misorientations between 30° and 60° represented more than 60% of the grains developed within the swirl zone.

The cold weld developed a finer structure throughout the weld nugget in both the transverse and normal directions than did the hot weld. Figure 6 demonstrates the grain size distribution and misorientation angle histograms, within the swirl zone for both hot and cold welds. An average grain size of 2.2 μm was measured for the cold weld compared with a 2.6 μm grain size for the hot weld. These are finer than the base metal. The misorientation angle histograms shown in Fig. 6 revealed that the finer structure in the cold weld was associated with a relatively high number fraction of low angle boundaries compared with the hot weld. Figure 7 shows the misorientation angle histogram for the base metal microstructure. The misorientation angle measured reveals the presence of a structure with low-angle boundaries ranging between 5° and 15°, while a large number fraction of boundaries has misorientation varying between 30° and 60°.

3.2 Superplastic Behavior

The superplastic behavior of the base metal and the FSW material welded at 2.1, 3.2, and 4.2 mm/s was investigated at a temperature of 495 °C and tensile strain rates ranging from

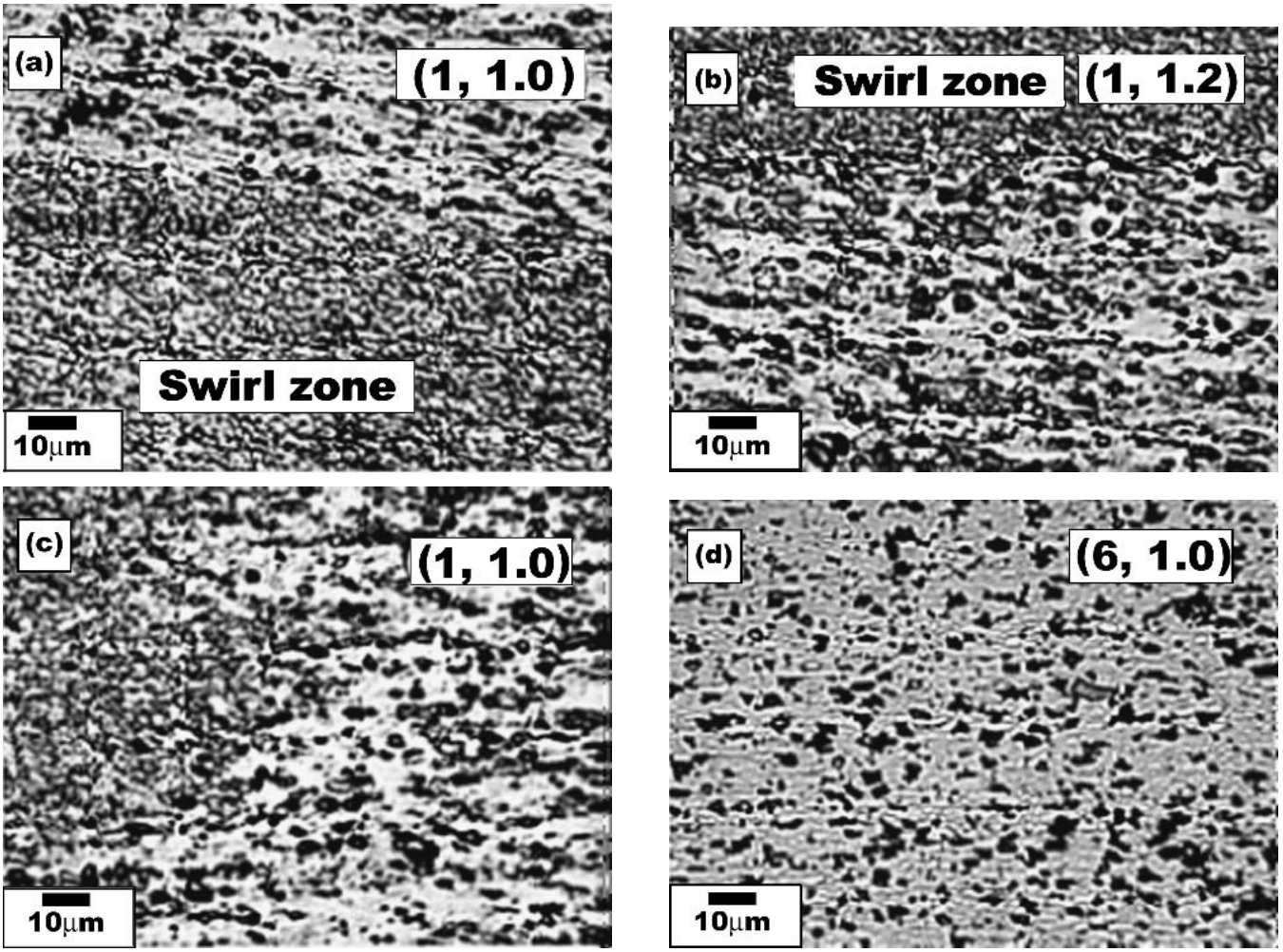

Fig. 4 Optical micrographs showing the various zones after welding: **(a)** at the top of the swirl zone, **(b)** at the bottom of the swirl zone, **(c)** in front of the swirl zone on the retreating side, and **(d)** at 1mm to the right of the retreating shoulder.

10^{-4} to 10^{-2} s^{-1}. Estimates of true-stress and true-strain were determined from force and elongation measurements using the assumptions of constant volume and uniform cross-sectional area change. Figure 8(a) shows typical stress-strain curves behavior at 495 °C and a strain rate of 10^{-3} s^{-1} for all three welded conditions. The sheets welded at 4.2 mm/s (cold welds) displayed a uniform constant flow stress of 8.8 MPa over the entire deformation path with the highest strain-to-failure of 1.9 (true strain). Sheets welded at an intermediate welding rate of 3.2 mm/s displayed a strain hardening behavior up to true strains of 0.4 followed by softening up to failure at 1.7. Similar behavior was displayed by the sheets welded at 2.1 mm/s (hot weld) but at relatively lower flow stresses for the same strain-to-failure. The base metal displayed a similar behavior to that of the hot welds, but had a higher flow stress of around 10 MPa with a stain-to-failure of 1.75. A similar superplastic behavior was reported by Kridli et al., who worked with alloy W049.[12] Here the higher welding rate was associated with a higher strain-to-failure and more constant flow stresses. Figure 8(b) shows the super plastic behavior of the friction stir welded sheets at 4.2 mm/s at 495 °C at different strain rates ranging between 10^{-4} and $10^{-2}s^{-1}$. From the diagram it is shown that the best strain rate is 10^{-3} s^{-1}. Deformation at strain rates of 10^{-2} s^{-1} resulted in a significant deterioration in the superplastic properties of the welded joints. Figure 9(a) shows a macrograph of the specimens tested at the optimum strain rate of 10^{-3} s^{-1}. It is observed that a uniform plastic deformation occurred during SPF over the entire gage length for all three welding rates. However, the 4.2 mm/s welds tested at different strain rates experienced a non-uniform deformation, especially at the lowest strain rates (10^{-4} $s^{\times-1}$), as shown in Fig. 9(b).

Figure 10 shows the effects of SPF strain rates on the percent elongation-to-failure and the maximum flow stress for the friction stir welded sheets at the welding rate of 4.2 mm/s before and after welding. The maximum superplastic elongations were achieved at 10^{-3} s^{-1} and 3×10^{-4} s^{-1} for the welded and un-welded sheets, respectively (Fig. 10a). A 570% elongation-to-failure was achieved at a strain rate of 10^{-3} s^{-1} with almost no change in flow stresses for the welded and unwelded sheets. Both welded and un-welded sheets lost their superplasticity at strain rates of 10^{-2} s^{-1}. The strain rate sen-

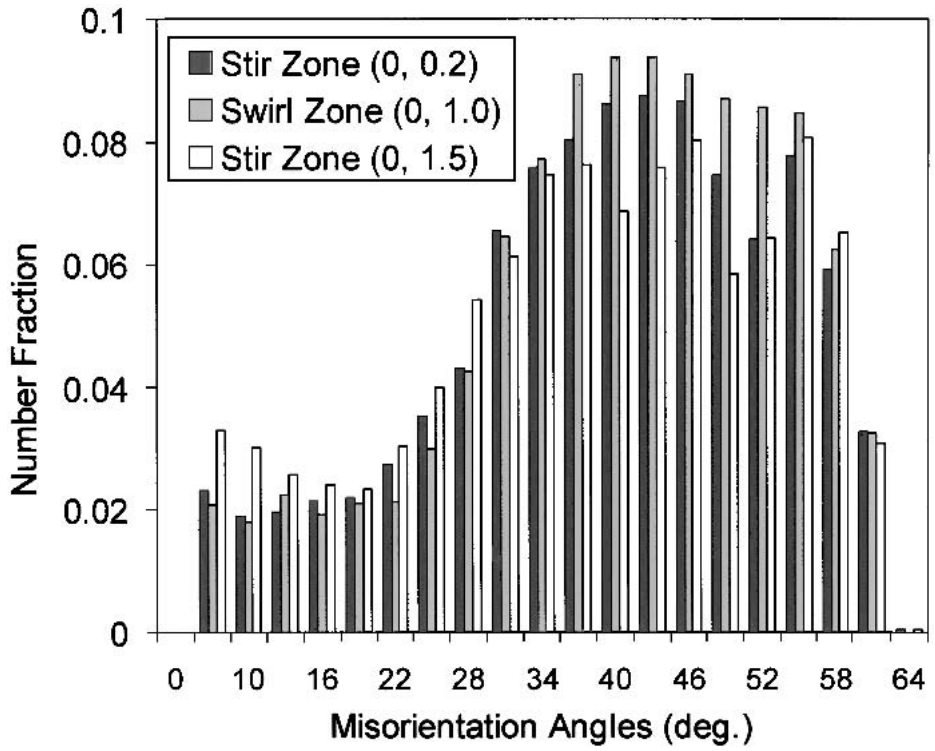

Fig. 5 Diagrams showing the misorientation angle histograms for the hot weld within the weld nugget center as a function of distance from the surface of the sheets

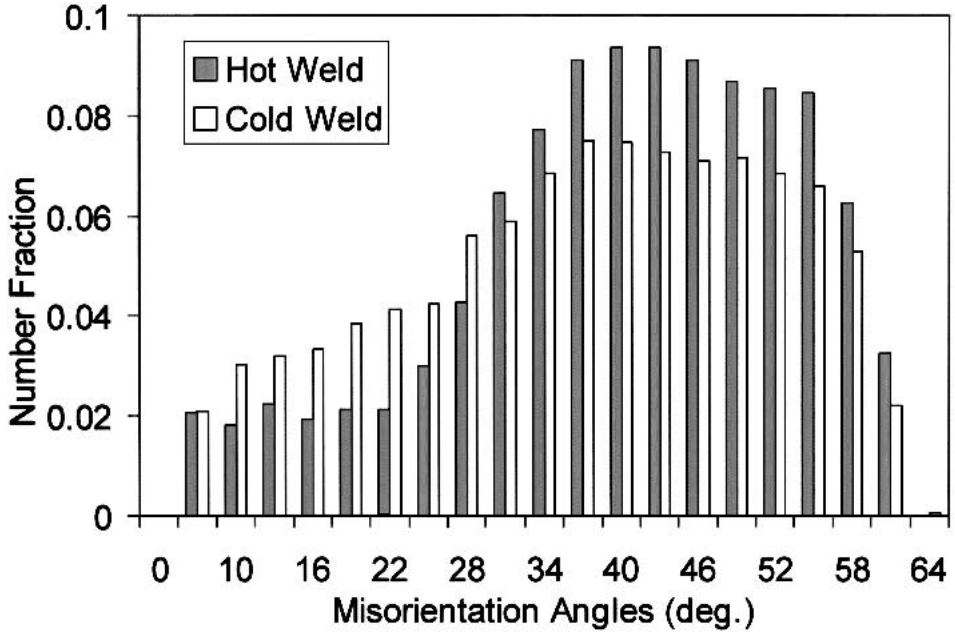

Fig. 6 Diagrams showing the misorientation angle histograms within the swirl zone for the hot and cold friction stir welding sheets

sitivity (m) was calculated by plotting flow stress against strain rate for different strains up to failure (Fig. 10b). The results showed that for the tested conditions, the average strain rate sensitivities were about 0.45 for the 4.2 mm/s weld and 0.52 for the base metal over strain rates of 10^{-4} to 10^{-3} s^{-1}.

4. Discussion

The swirl zone in the friction stir weld nuggets was smaller than the stir zone. It appeared only at a depth of about 0.8 mm from the surface of the sheet and was terminated above the

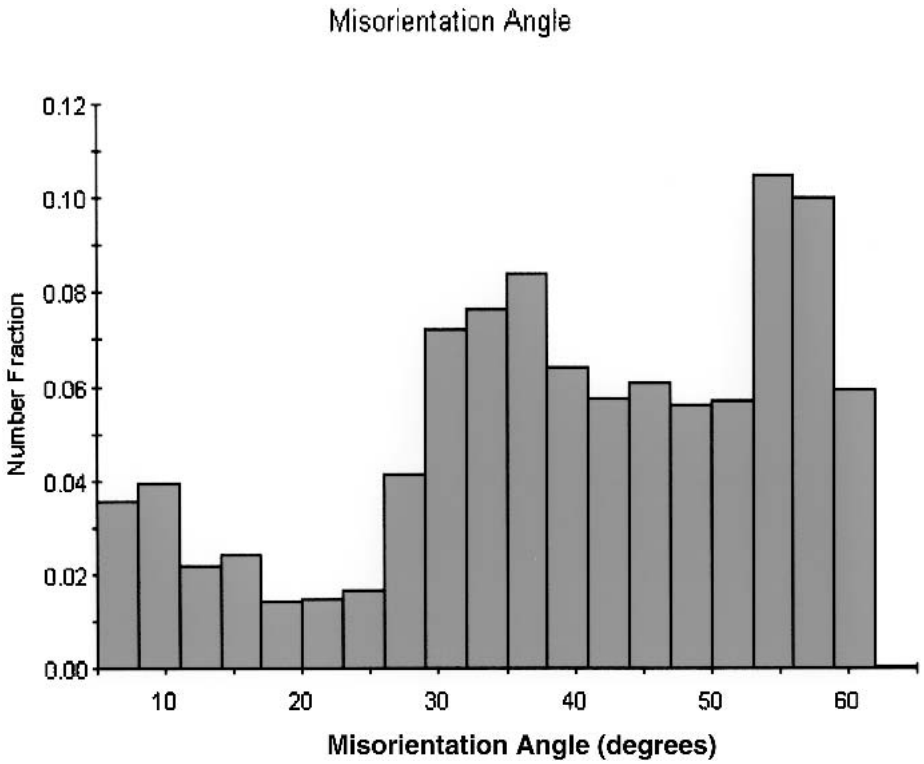

Fig. 7 Diagrams showing the misorientation angle histograms of the as-received dynamically recrystallized (DRX) sheets

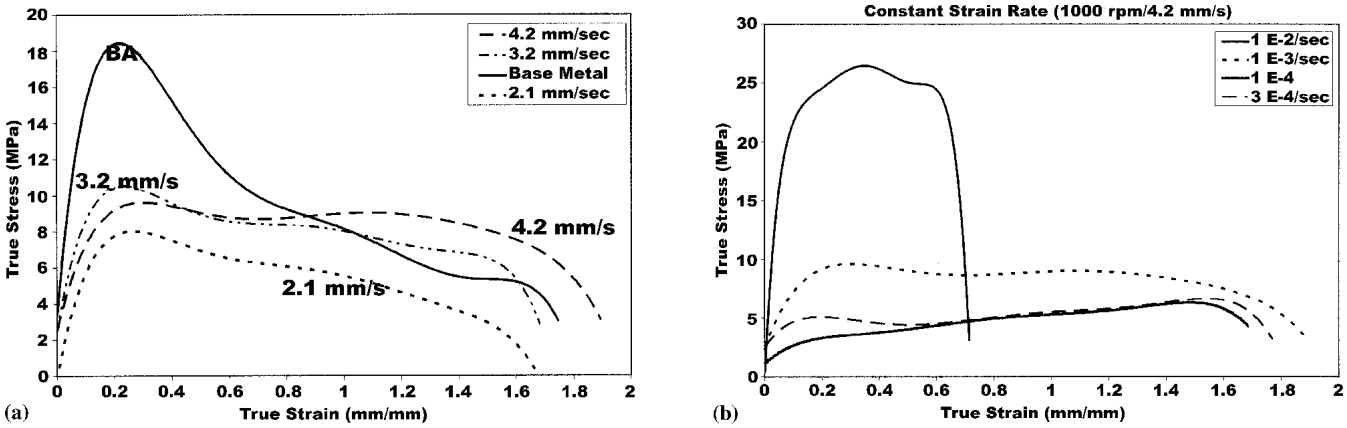

Fig. 8 True stress-true strain super plastic behavior of the friction stir welded sheets at 1000 rpm **(a)** at welding rate of 2.1, 3.2, and 4.2 mm/s compared with base metal, and **(b)** 1000 rpm and 4.2 mm/s welding rate at different strain rates

bottom surface by about 0.15 mm (Fig. 3). The heat lost to the anvil supporting the bottom of the sheets resulted into a temperature gradient that could be attributed to this observation. Similar observations were made by Mishra et al., who worked with 7075Al and 2519 alloys.[13] Inhomogenity in the microstructure was also observed across the width of the weld nugget. This may be related to greater heat generated at the retreating side of the weld due to shoulder friction with the sheet surface, resulting in greater softening of the retreating side material and hence a relatively coarser structure.

After friction stir welding, the non-uniform as-received structure of equiaxed and pancake-shaped grains was replaced by finer equiaxed structure in the swirl zone of the hot weld. The OIM misorientation analysis revealed that friction stir welding increased the grain boundary misorientation. This agrees with the findings of Jata et al., who investigated the effect of friction stir welding and processing on Al-Li-Cu alloy.[14] Jata suggested that a continuous dynamic recrystallization by dislocation-glide-assisted-subgrain-rotation occurs during friction stir welding since the strain rates are too high to allow for subgrain rotation by boundary sliding. However, this mechanism might not be applicable for materials with an initial structure that is already dynamically recrystallized. Dynamic recovery or extended recovery could be the dominating mecha-

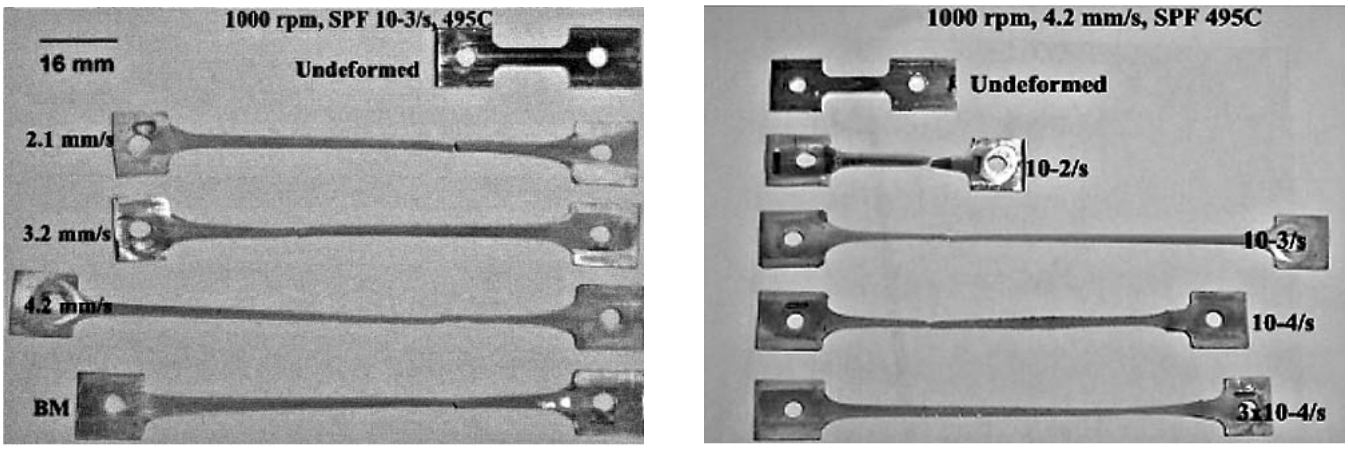

Fig. 9 Macrographs showing the superplastic tensile tested specimens: (a) friction stir welded sheets at different welding rates, SPF at 495 °C, and constant strain rate of 10^{-3} s^{-1} compared with base metal and **(b)** friction stir welded sheets at 4.2 mm/s at constant strain rates of 10^{-2} to 10^{-4} s^{-1}.

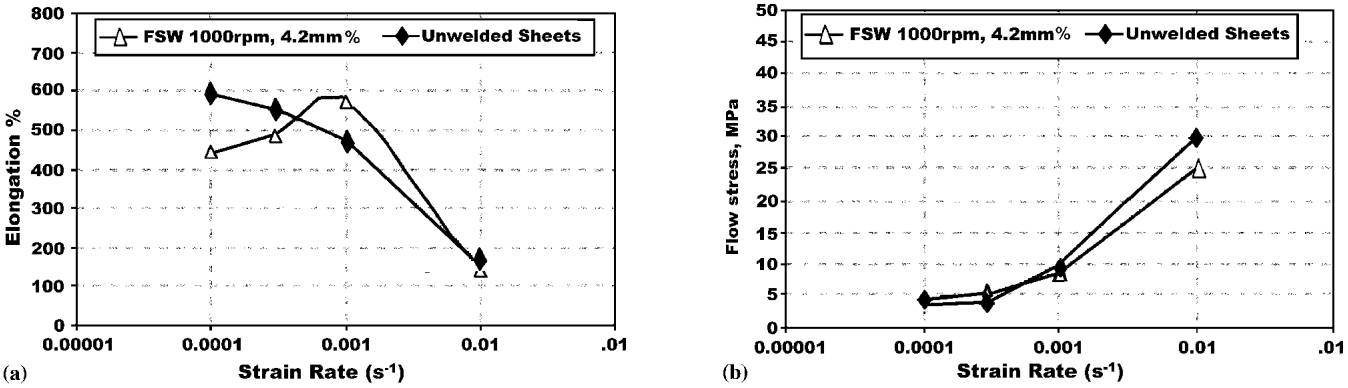

Fig. 10 Diagrams representing the strain rate variation for the 2095 sheets before and after welding 4.2 mm/s welding rate as a function of **(a)** percent elongation and **(b)** flow stresses.

nism, however, further analysis and investigations are necessary to conclusively determine which mechanism dominates. Due to the material flow around the pin within the stir zone to about 2 mm on either side of the weld nugget center, the coarse second phase particles were fragmented into finer particles. Regions closer to the surface (above the swirl zone) were subjected to higher temperatures and hence greater dissolution of second phase particles. Material moved down by the rotating pin dragged the fragmented particles and fine precipitates with it toward the swirl zone. This could explain the observed particle segregation within the swirl zone, which agrees with the findings of Salem.[15] This also agrees with the observations, made by Meyer et al., who investigated the behavior of friction stir welding Al-Mg-Si-Cu Al alloys.[16] Higher welding rates resulted in lower heat input during welding.[17,18] The lower the deforming temperature (i.e., higher welding rate), the higher the intensity of plastic deformation within the the swirl zone, and hence, the higher the fraction of low-angle boundaries. This is indicative of the early stages of dynamic recovery, which produces a structure with low angles of misorientation.[19]

Previous research that was carried out on the superplastic behavior of friction stir welding 2095 in direction transverse to the weld indicated that, while friction stir welding retained the superplastic properties of the material, the deformed specimens showed non-uniform deformation across the weld nugget. This was due to the structural differences between the various weld zones. The current study focused on the super plastic behavior of the stir zone. Not only did friction stir welding retain the superplasticity of the original Weldalite 2095 sheet, but it also produced a structure with higher strain rate superplasticity. The superplastic behavior, investigated as a function of strain rates of 10^{-4} s^{-1} to 10^{-2} s^{-1} at a deforming temperature of 495 °C, obtained a maximum superplasticity at $10^{-3}s^{-1}$ for the cold weld. For this weld, elongation-to-failure was about 100% higher than that of the un-welded sheets. Further investigation should be made to understand the behavior of the second phase particles before and after superplastic forming at 495 °C. It is possible that segregation of fine coherent $\beta'(Al_3Zr)$ precipitates within the swirl zone could have increased the stability of the structure against grain growth and hence improved the superplastic behavior of the cold welds. Such particles are too small to be revealed by optical microscopy. In addition, the fine equiaxed structure developed by friction stir welding at the highest welding rate could have evolved into a higher angle

boundary structure by dynamic recovery during the equilaberation time at 495 °C before tensile testing starts. According to Jata et al.[14] the extensive plastic deformation and thermal effect induced within the stir zone lead to contineous recovery and dynamic recrystallization, which agrees with the current suggestions. This could have resulted in the improved superplastic behavior of the cold welds.

5. Conclusions

Friction stir welding was used to join dynamically recrystallized superplastic Weldalite sheets. Friction stir welding developed a fine equiaxed high angle boundary structure within the swirl zone. The higher welding rate produced a more uniform fine-grained equiaxed structure with a uniform distribution of fine particles around the weld nugget center, which increased the stability of the microstructure during elevated temperature testing. The highest level of superplastic elongation (>570%) was achieved at a deforming temperature of 495 °C and a constant strain rate of 10^{-3} s^{-1}. Results indicate that friction stir welding is capable of shifting the SPF strain rate of the Weldalite by one order of magnitude higher as well as increasing the strain-to-failure by 20%. This is a significant improvement in superplastic behavior.

Acknowledgments

This material is based upon work supported by the National Science Foundation under Grant No. 0108894. The technical assistance of Dr. Wei Tang and Mr. Dan Wilhelm at the University of South Carolina and Mr. M. Attallah and Mr. R. Baher at American University in Cairo is gratefully acknowledged.

References

1. G. Biallas, R. Braun, C. Donne, G. Staneik, and W. Kaysser: "Mechanical Properties and Corrosion Behavior of Friction Stir Welded 2024-T3" in *1st International FSW Symposium*, The Welding Institute, ed., Abington Hall, UK, 14-16 June 1999, Rockwell Science Center, Thousand Oaks, CA.
2. C. Donne and G. Biallas, T. Ghidine, and G. Raimbeaux: "Effect of Weld Imperfections and Residual Stresses on the Fatigue Crack Propagation in Friction Stir Welded Joints," in *2nd International Conference on Friction Stir Welding,* The Welding Institute, ed., Abington Hall, UK, 26-28 June 2000, Gothenburg, Sweden, on CD-Rom.
3. R.S. Mishra and M.W. Mahoney: "Friction Stir Processing: A New Grain Refinement Technique to Achieve High Strain Rate Superplasticity in Commercial Alloys," *Mat. Sci Forum*, 2001, *357-359,* pp. 507-14.
4. Z. Ma, R. S. Mishra, and M. W. Mahoney: "Friction Stir Processing for Microstructural Modifications of an Aluminum Casting," *Acta Materiala*, 2002, *50,* pp. 2219-30.
5. H.G. Salem, A. Reynolds, and J. Lyons: "Microstructure and Retention of Superplasticity of Friction Stir Welded Superplastic 2095 Sheets, *Scripta Met*., 2001, *45*(5), pp. 337-342.
6. H.G. Salem, A. Reynolds, and J. Lyons: "Effect of Friction Stir Welding on the Superplastic Behavior of Weldalite Alloys," in *Lightweight Alloys For Aerospace Applications*, K. Jata, E.W. Lee, W. Frazier, and N.J. Kim, ed., TMS, Warrendale, PA, 2001, pp. 141-50.
7. H. Salem, R. Goforth, and T. Hartwig: "Influence of Intense Plastic Straining on Grain Refinement, Precipitation, and Mechanical Properties of Al-Cu-Li base Alloys," *Metall. Mater. Trans. A,* 2003, *34A*(5), pp. 1153-61.
8. T. J. Lienert, W. L. Stellwag, and L. R. Leham: "Microstructural Evolution in Friction Stir Weldon 6061-T651," in *1st International FSW*, 14-16 June 1999, Rockwell Science Center, Thousand Oaks, CA.
9. M. Posada, J. Deloach, A. Reynolds, M. Skinner and J. Halpin: "Friction Stir Weld Evolution of DH-36 Stainless Steel Weldments" in *Friction Stir Welding and Processing II, TMS 2001,* V. Jata, M.W. Mahoney, R.S. Mishra, S.L. Semiatin, and D.P. Field, ed., pp. 159-72.
10. M. Mahoney, R. Mishra, T. Nelson, J. Flintoff, R. Islamgalliev and Y. Hovansky: "High Strain Rate, Thick Section Superplasticity Created via Friction Stir Processing," *TMS 2001, Friction Stir Welding and Processing II*, Ed. K. Jata *et al*., pp. 183-93.
11. G. Oertelt, S. Babu, S. David, and E. Kenik: "Effect of Thermal Cycling on Friction Stir Welds of 2195 Aluminum Alloy," *Welding Research Suppl.*, March 2001, pp. 71s-79s.
12. R. S. Mishra., R. K. Islamgalliev, T. W. Nelson, Y. Hovansky, and M. W. Mahoney: "Abnormal Grain Growth During High temperature Exposure in Friction Stir Processed 7075 and 2519 Aluminum Alloys" in *Friction Stir Welding and Processing,* V. Jata, M.W. Mahoney, R.S. Mishra, S.L. Semiatin, and D.P. Field, ed., TMS, Warrendale, PA, 2001, pp. 205-15.
13. G. T. Kridli, A. S. El-Gizawi and R. Lederich: "Development of Process Maps for Superplastic Forming of Weldalite™ 049," *Mater. Sci and Eng. A,* 1998, *A244,* pp. 224-32.
14. K.V. Jata and S.L. Semiatin: "Continuous Dynamic Recrystallization During Friction Stir Welding of High Strength Aluminum Alloys," *Scripta Mater*., 2000, *43,* pp. 743-49.
15. H.G. Salem: "Friction Stir Weld Evolution of Dynamically Recrystallized AA 2095 Weldments," *Scripta Materialia*, 2003, *49*(11), pp. 1103-10.
16. C. Meyer, H. Doyen, D. Emanowski, G. Tempus, T. Hirsch, and P. Mayer: "Dispersoid-Free Zones in the Heat-Affected Zone of Aluminum Alloy Welds," *Metall. Mater. Trans. A*, 2000, *31A,* pp. 1453-59.
17. A.P. Reynolds, T.V. Seidel, and M. Simonsen: "Visualization of Material Flow in Autogenous Friction Stir Weld" in *1st International FSW Symposium*, The Welding Institute, ed., Abington Hall, UK, 14-16 June 1999, Rockwell Science Center, Thousand Oaks, CA.
18. J.E. Mitchell, G.E. Cook, and A.H. Strauss: *1st International FSW Symposium*, The Welding Institute, ed., Abington Hall, UK, 14-16 June 1999, Rockwell Science Center, Thousand Oaks, CA.
19. F. J. Humphreys and M. Hatherly, *Recrystallization and Related Annealing Phenomena*, 1st ed., Elsevier Science Ltd., Amsterdam, The Netherlands, 1995.